CFD Simulation of a Free-Surface Isothermal Water Flow in the MYRRHA target geometry (MYRRHA Benchmark)

L. Maciocco

December 2002

Abstract

The simulation of the MYRRHA free-surface water experiment using an Arbitrary Eulerian-Lagrangian Moving Mesh Algorithm implemented in the Star-CD commercial CFD code is presented.

In spite of the complexity of the surface morphology, relatively to this type of approach for free surfaces modelling, results show that the algorithm is able to give quantitatively correct results in terms of velocity profiles. Although no measurements of the surface shape are available, it can be guessed that it is well predicted.

Better results are obtained without taking into account surface tension, whose effects seem to be overestimated, probably due to the presence of surface discontinuities in the real free surface.

Contents

1 Introduction....3
2 Test case set-up....4
2.1 Description....4
2.2 Numerical set-up and boundary conditions....5
2.3 Calculation strategy....6
3 Results....7
3.1 Results for case 1-a (no surface tension)....7
3.2 Results for case 1-b (with surface tension)....10
4 Conclusions....13
5 References....13

1 Introduction

In the framework of the R&D activity related to high-power spallation targets design, the windowless concept is considered a very promising alternative to the classical approach, where the spallation material (liquid metal, LM) is separated from the high-vacuum beam line by a solid interface (window). In the windowless concept, the free surface of the flowing LM is directly exposed to the proton beam; this is possible thanks to the very low vapour pressure of liquid metals (for example, the value of the PbBi vapour pressure at 200 °C is $p_v = 1.51 \times 10^{-11}$ Pa).

Due to the very high and non-homogeneous heat fluxes generated by the spallation process, a detailed thermal-hydraulic CFD simulation is a necessary step for the design of an efficient spallation target. This is especially true for the windowless approach, where the correct prediction of the free-surface shape and the corresponding velocity and temperature fields is crucial to avoid stagnation regions within the spallation zone which, due to the high power generated by the spallation process (~ 200 W/cm^3/mA), would result in the boiling of the LM. Also, in order to have a stable neutron source, the level and the shape of the free surface should be stationary, i.e. free surface instabilities should be avoided.

However, the state of the art of numerical modelling of free surface flows is not so advanced as in the case of one-phase flows, even in the case of common fluids like water and air [1]. The most common CFD approaches to free-surface flow modelling are based on the Volume of Fluid (VOF) method, which tracks the free surface evolution through the solution of a transport equation for an active scalar. Usually, commercial codes like STAR-CD, FLUENT and CFX integrate the VOF method in a two-phase approach, where both the light and the heavy fluids are modelled. Other codes, like FLOW-3D, couple the VOF method with a boundary reconstruction technique, hence modelling only the heavy fluid and treating the free surface as a constant-pressure boundary. This assumption is well justified in many industrial applications and is especially true in the case of heavy liquid metals.

In spite of the capability of the VOF method to face even very complex free-surface evolutions, it presents some drawbacks. The main problem of the VOF approach is the tendency to smearing the interface, which is contrasted by using special advection schemes and interface-sharpening algorithms which, however, could alter the surface dynamics. In the case of two-phase approaches, further physical and numerical limitations arise [1].

An alternative approach was followed at CRS4, based on an arbitrary Eulerian-Lagrangian moving-mesh method, which has been implemented in the STAR-CD code taking advantage from its moving-mesh capabilities [2]. The free surface is simulated as a constant-pressure moving boundary, where vertical displacements of each boundary face are assigned according to a height-function concept. Although more limited than the VOF method regarding surface-shape complexity, it presents some advantages in terms of simplicity and accuracy, and allows an easy implementation of both heat and mass exchange processes at the interface.

The Moving Mesh Algorithm (MMA) described above has already been successfully validated on two standard case (rotating cylinder and surface sloshing), the analytical solution was known for, and has been tested on 2D and 3D test cases typical of spallation target systems. The simulation of the MYRRHA water experiment performed by SCK-CEN in the framework of the MYRRHA windowless target design and proposed for the ASCHLIM activity [3], is presented in this document.

2 Test case set-up

2.1 Description

The test case consists of an isothermal water flow downcoming along an annular channel and converging in a pipe, forming at the top a free surface at atmospheric pressure [3]. The geometry of the test section is shown in Figure 1. A flow guide separates the annular downcomer from the central tube with air at atmospheric pressure. The flow enters the downcomer from an annular collector across a row of antiswirl blades and through a smoothing grid, which is placed about 200 mm upstream the end of the flow guide, considered as the reference level.

Water physical properties at the experimental temperature (30 ^{o}C) are listed in Table 1; the experimental conditions proposed for the benchmark exercise are listed in Table 2. For cases 1 and 3 the free surface position in still conditions coincides with the reference level, while in case 2 it is assumed to be 10 mm below the reference level, corresponding to a the extraction of 4.07×10^{-5} m^3 of water.

Experimental LDV profiles of axial and azimuthal (tangential) velocity components and their fluctuations are available in 7 sections, listed in Table 3.

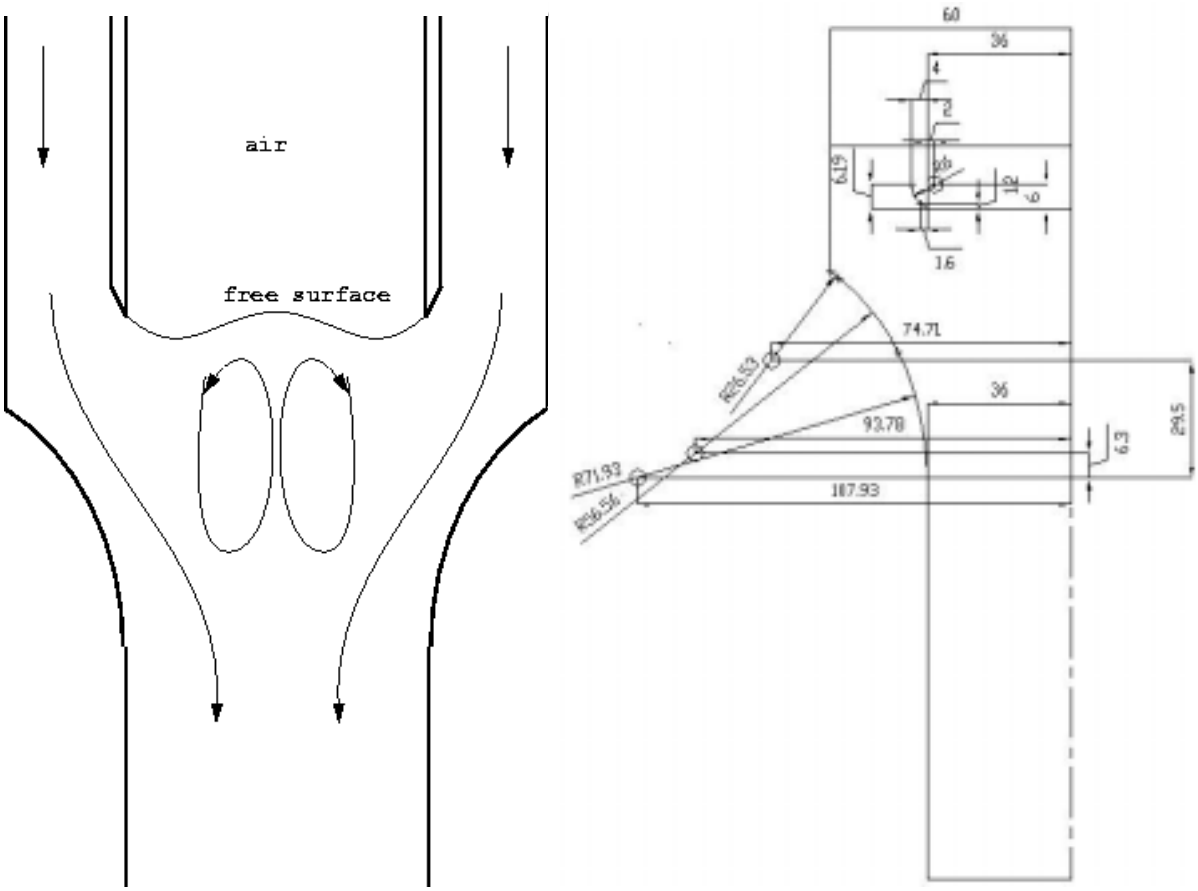

Figure 1 - Sketch and exact geometry of the MYRRHA water experiment test section.

Table 1 - Water physical properties at T = 30 °C.

Density ρ (Kg/m^3)	995.62
Viscosity μ (Kg/ms)	7.985×10^{-4}
Cinematic viscosity ν (m^2/s)	8.02×10^{-7}
Surface tension γ (N/m)	7.12×10^{-2}

Table 2 - Experimental conditions.

Case	Flow rate (l/s)	Mean inlet velocity (m/s)	Re	Free surf. position (mm)
1	5	0.796	4.0×10^4	0
2	5	0.796	4.0×10^4	-10
3	6.8	1.082	5.4×10^5	0

Table 3 - Position of experimental cross sections

Section	z position (mm)
1	+20
2	+15
3	+10
4	-5
5	-7.5
6	-10
7	-12.5

2.2 Numerical set-up and boundary conditions

The computational domain and the computational mesh in the free-surface region are shown in Figure 2. Inlet (red with yellow arrows), outlet (green) and the pressure boundary condition corresponding to the free-surface (orange) are also shown. Cyclic boundary conditions are applied on side walls. A mixed structured-unstructured was used mesh with a total number of about 12000 cells.

The Moving Mesh Algorithm (MMA) [2] was used to simulate the free surface dynamics. The moving cells in the computational domain are plotted in red in Figure 2; hexahedral elements are compulsory in this region.

Due to the topology of the free surface, the detachment point of the free surface must be bonded to the end of the flow guide. This is a limitation to the real behaviour of the free surface, whose detachment point could change with the flow conditions. However, according to experimental observations, the displacements of the detachment point from the reference position should be limited (at list for cases 1 and 3), so that this assumption might not introduce significant errors.

All simulations were transient run integrated with the PISO algorithm. The MARS second-order [5] and the Upwind first order schemes were applied to the momentum and turbulence equations respectively. The Chen k-ε model [5] [6] with Wall Functions was used.

In order to avoid pressure shocks, leading to wave braking and then to the MMA failure, in all the simulations the inlet mass flow rate was increased with a ramp from zero to the final value during the first 2 seconds of run.

Surface tension is modelled through the application on the free surface of a pressure load proportional to the surface curvature.

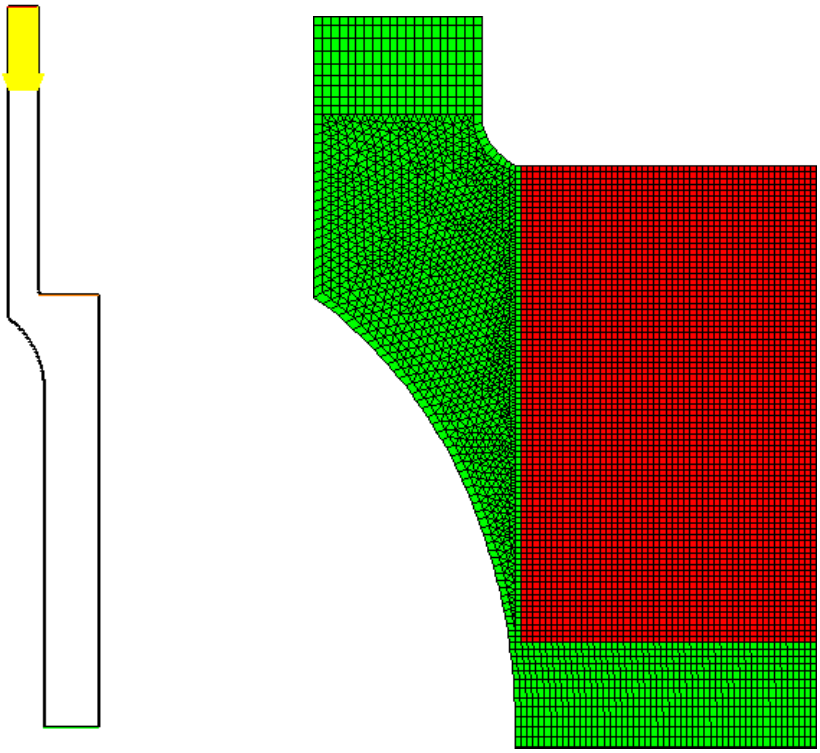

Figure 2 - Computational domain with the boundary conditions (left) and computational mesh in the free-surface region.

2.3 Calculation strategy

Two cases were simulated, both corresponding to experimental case 1, with and without surface tension (Table 4). The assumption of bonded surface detachment point was considered too strict for a correct simulation of case 2.

Table 4 - List of test cases.

	Experimental conditions	**Surface tension**
Case 1-a	Case 1	NO
Case 1-b	Case 1	YES

3 Results

3.1 Results for case 1-a (no surface tension)

The simulation was carried out for 9 s, when a quasi-steady solution was obtained. This is shown in Figure 3, where the free surface evolution during the last second of simulation is presented.

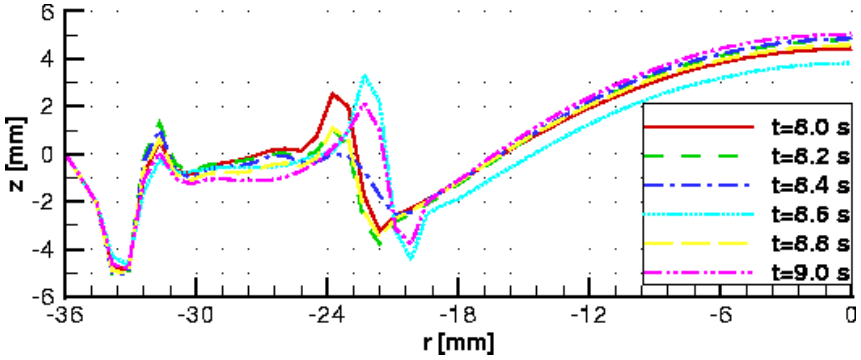

Figure 3 - Case 1-a: free surface shape evolution during the last second of simulation.

Velocity and static pressure fields at the end of the simulation are shown in Figure 4. As expected, a big recirculation zone is generated in the central core. A secondary stagnation region is generated beside the surface detachment point. Due both to the influence of the bonded detachment point and to the resulting surface shape, which presents two sharp cusps with a very distorted mesh (see also Figure 5), it is the author opinion that the free surface shape in this zone is only qualitative.

The comparison between experimental and calculated axial velocity profiles along the cross sections reported in Table 3 (and also sketched in Figure 4) is presented in Figure 6. In order to estimate the effect of the flow unsteadiness on velocity profiles, calculated results are reported at two different times (8.6 s and 9 s), corresponding to the two most different free surface shapes observed during the last second of simulation (see Figure 3). No significant differences arise in general between the two velocity profiles, apart from a velocity peak at half section 4 (and in section 5 in smoother way) at t=8.6 s, probably generated by a sudden change of the free surface shape in the stagnant zone.

A good agreement with experimental profiles can be observed in all sections, confirming a correct reproduction of the flow pattern and, as a consequence, of the free surface shape. Some differences can be observed in section 1,2 and 3, where experimental profiles already show an irregular shape, probably due the effect of the anti-swirl blades placed at the beginning of the annular channel [4], which can not be reproduced by the simulation. The effects of these irregularities is still present in downstream sections 4 - 7 as a layer of slower fluid near the outer wall, and a consequent slight increase of the velocity magnitude in the central part of the main stream. In spite of this fact, the shear layer between the main stream and the central recirculation region is well reproduced by the simulation in all sections but section 4, soon after the free surface detachment point. Here, experimental results show a steeper velocity profile, possibly revealing a slightly different position of the free-surface detachment point with respect to inner edge of the flow guide, which is imposed in the simulation. The tendency to an earlier detachment of the surface can be also deduced from

the surface shape near its starting point (Figure 9). In fact, it tends to go immediately down, revealing a depression which could lead to an anticipated flow detachment.

Experimental and numerical profiles of turbulence intensity, calculated as $q = \sqrt{2k}$, are plotted in sections 1 and 7 in Figure 7. A strong discrepancy can be observed, which is in contrast with the very good agreement of velocity profiles. No definite explanation for such discrepancy was found, although it could be probably due to measurements or data-elaboration errors.

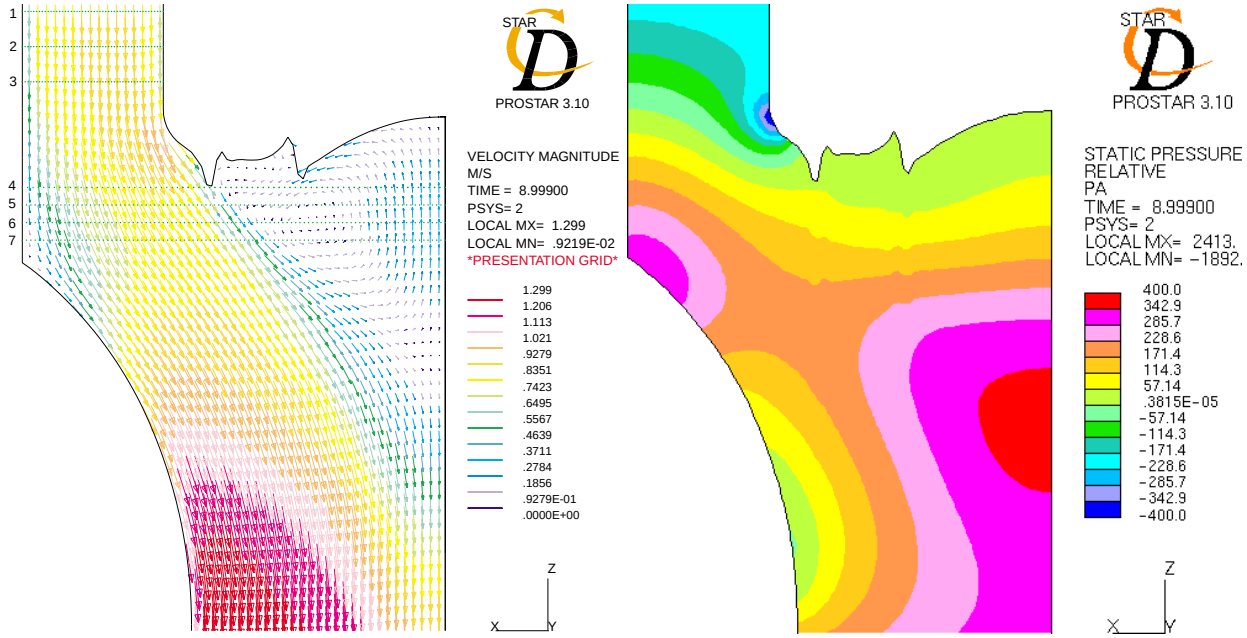

Figure 4 - Case 1-a: velocity (left) and static pressure (right) fields in the surface region at t = 9s. Probe sections for comparison with experimental results are also sketched.

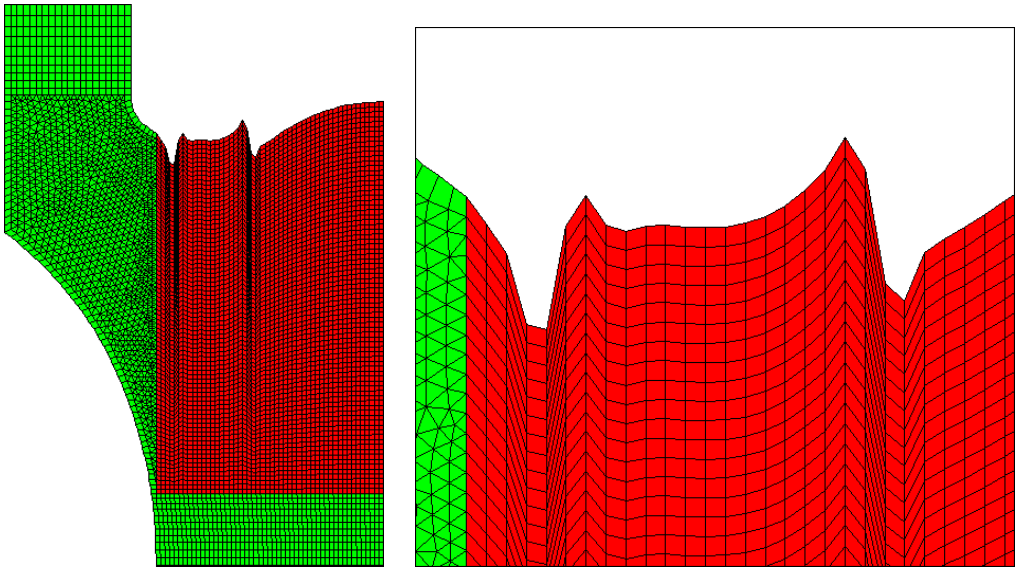

Figure 5 - Case 1-a: mesh displacement at t = 9s

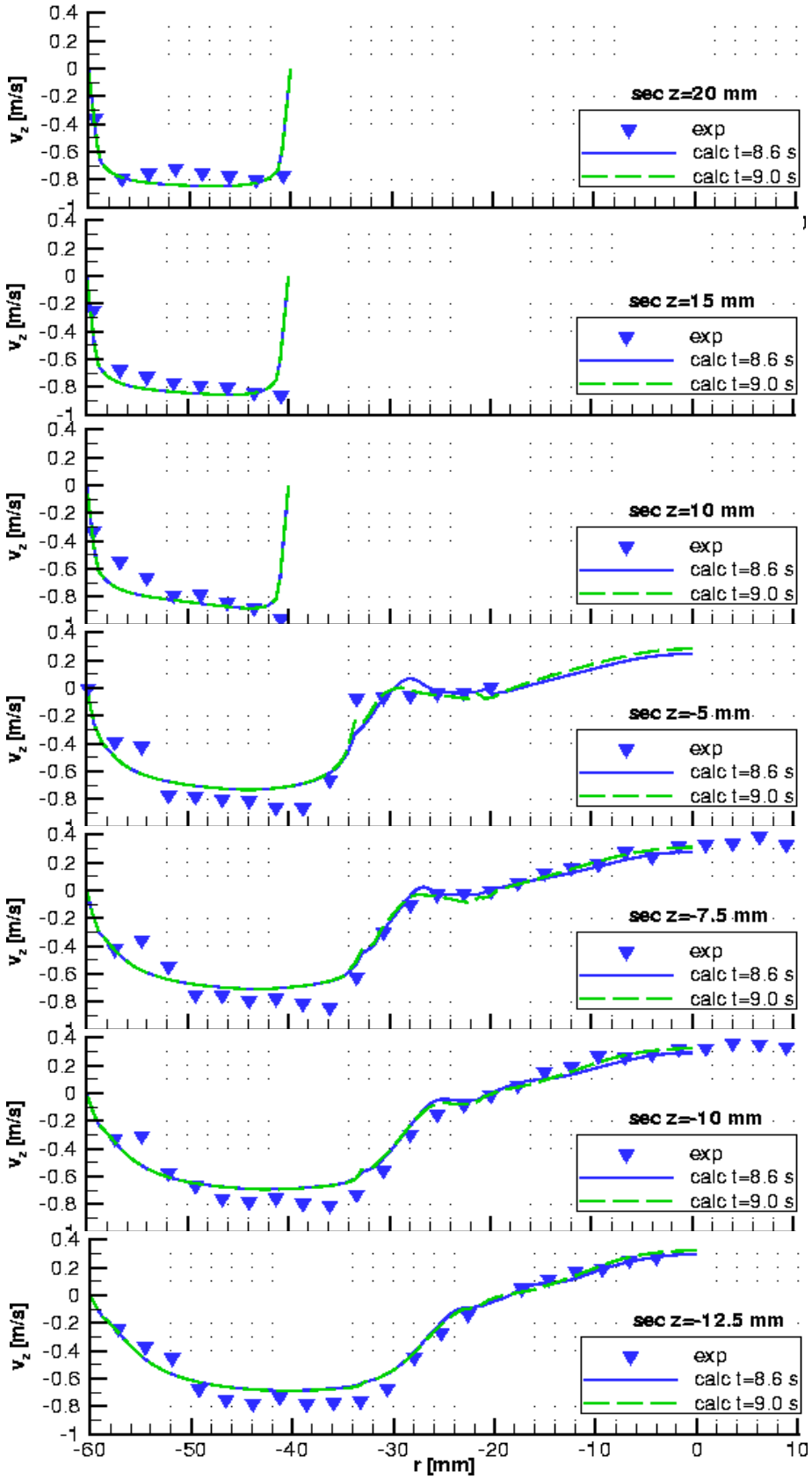

Figure 6 - Case 1-a: comparison between experimental and calculated axial velocity profiles in the prescribed sections.

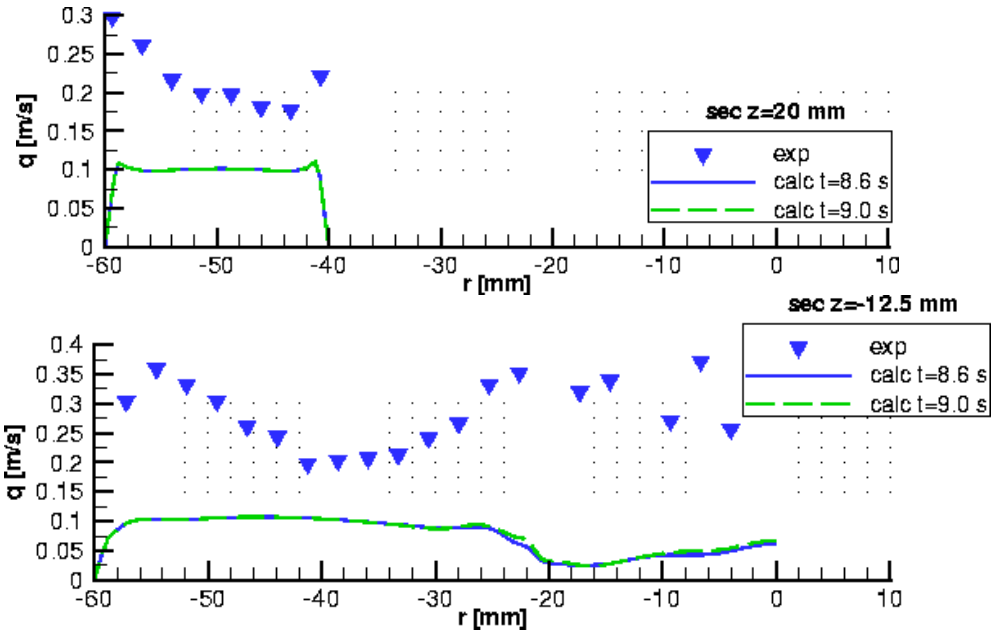

Figure 7 - Case 1-a: experimental and numerical turbulence intensity profiles in sections 1 and 7.

3.2 Results for case 1-b (with surface tension)

The simulation was run for 5 s, when a quasi-stationary solution was reached. Figure 8 shows the free surface evolution during the last second of simulation. Free surface oscillations are wider than in case 1-a, due to the elastic effect of surface tension, and the average maximum surface height is about 3 mm, while it was 4 mm in case 1-a.

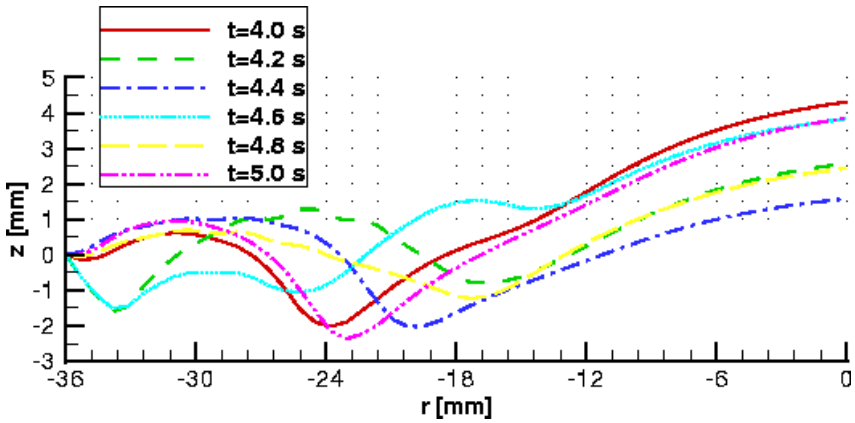

Figure 8 - - Case 1-b: free surface shape evolution during the last second of simulation.

As it can be observed in Figure 9, surface cusps are smoothed down by the effect of surface tension, so reducing mesh distortions (Figure 10). The pressure field generated by the surface tension on the surface at t=5 s is also shown in Figure 10.

The comparison with experimental velocity profiles still shows a reasonable agreement, although better results were obtained without the effect of surface tension. This implies that its effects are

overestimated in the simulation. This can be due the fact that the real surface is discontinuous in the stagnating zone between the main stream and the recirculation region, while in the simulation it must be continuous. This results in sharp wedge in the case 1-a, while in this case surface tension generates a strong depression, which raises the surface in this point, so lowering it in the centre.

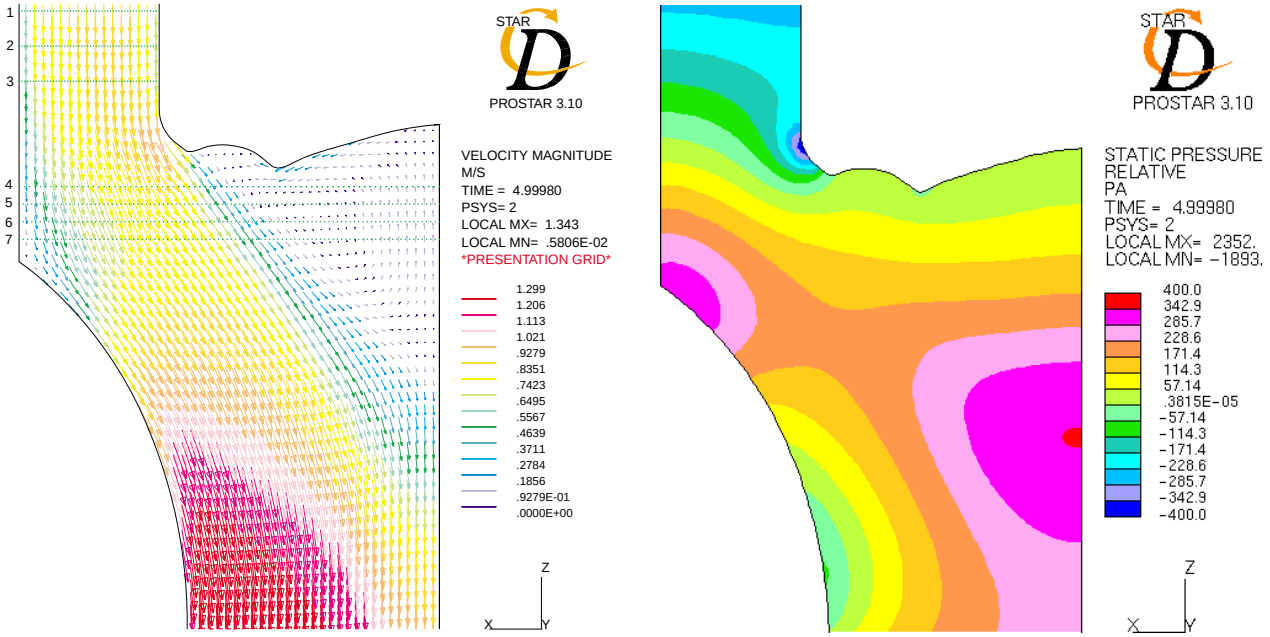

Figure 9- Case 1-b: velocity (left) and static pressure (right) fields in the surface region at t = 9s. Probe sections for comparison with experimental results are also sketched.

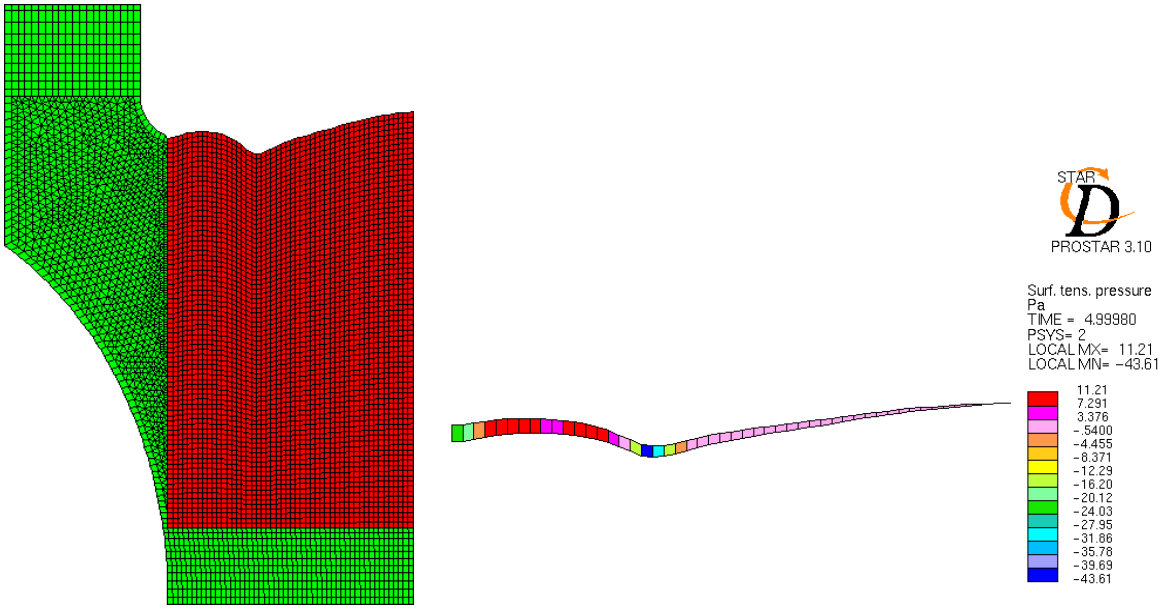

Figure 10 - - Case 1-b: mesh displacement at t = 5s (left) and corresponding surface-tension pressure on the free surface (right)

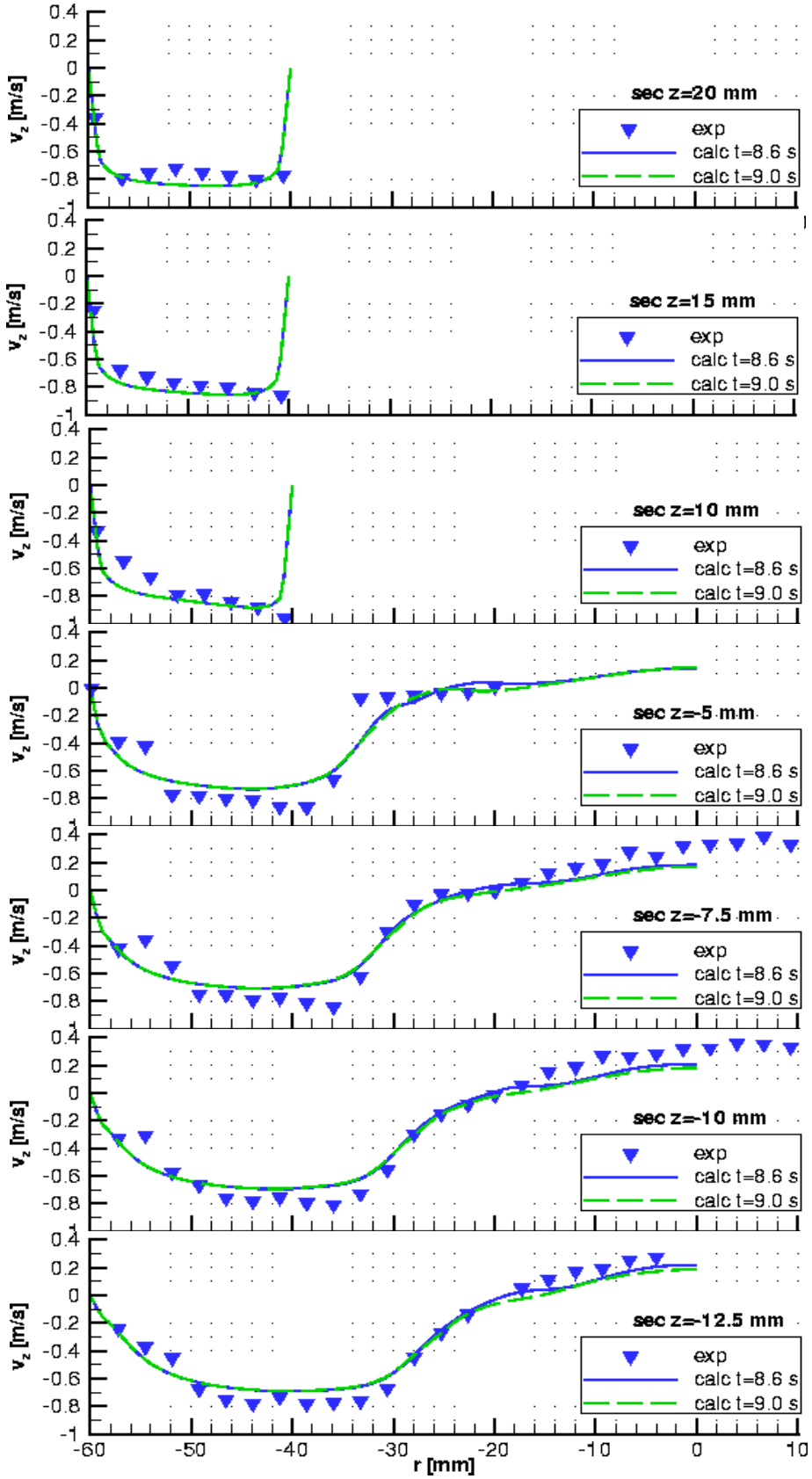

Figure 11 - Case 1-b: comparison between experimental and calculated axial velocity profiles in the prescribed sections.

4 Conclusions

The MYRRHA free-surface water experiment was simulated using an Arbitrary Eulerian-Lagrangian Moving Mesh Algorithm implemented in the Star-CD commercial CFD code.

In spite of the complexity of the surface morphology, relatively to this type of approach for free surfaces modelling, results showed that the algorithm is able to give quantitatively correct results in terms of velocity profiles. Although no measurements of the surface shape are available, it can be guessed that it is well predicted. A strong discrepancy was found in the comparison of turbulence level profiles, which has still to be explained.

Better results were obtained without taking into account surface tension, whose effects seem to be overestimated, probably due to the presence of surface discontinuities in the real free surface.

In conclusion, the MMA seems to be a very effective way to simulate free-surface flows typical of windowless spallation target.

5 References

[1] L. Maciocco et al., "*Review and Application to Windowless Spallation Targets of Free Surface Flow Models in Commercial Codes*", CRS4 Tech. Rep. 99/20, November 1999

[2] L. Maciocco, V. Moreau, "*Implementation of a Moving-Mesh Free-Surface Algorithm in Star-CD*", report in progress

[3] K. Van Tichelen, "*ASCHLIM WP8 - Myrrha Free-Surface Spallation Target Experiment - Input Description*", Reactor Physics & Myrrha SCK-CEN report, January 2002

[4] SCK-CEN information

[5] Star-CD v3.05 User Manual (Methodology volume), Computational Dynamics Limited, 1998.

[6] Y.S. Chen, S.W. Kim, “Computation of turbulent flows using an extended k-ε turbulence closure model”, NASA CR-179204, 1996